Dynamic simulation of non-spherical particulate suspensions

David Kittipoomwong, Howard See and Nam Mai-Duy

June 19, 2009

1 Abstract

Particle-level simulation has been employed to investigate rheology and microstructure of non-spherical particulate suspensions in a simple shear flow. Non-spherical particles in Newtonian fluids are modeled as three-dimensional clusters of neutrally-buoyant, non-Brownian spheres linked together by Hookean-type constraint force. Rotne-Prager correction to velocity disturbance has been employed to account for far-field hydrodynamic interactions. An isolated rod-like particle in simple shear flow exhibits a periodic orientation distribution, commonly referred to as Jeffery orbit. Lubrication-like repulsive potential between clusters have been included in simulation of rod-like suspensions at various aspect ratios over dilute to semi-dilute volume fractions. Shear viscosity evaluated by orientation distribution qualitatively agrees with one obtained by direct computation of shear stress.

Keywords: particle-level simulation, fiber, suspension rheology, shear-induced diffusion

2 Introduction

Non-spherical particulate suspensions are commonly found in both natural and man-made materials such as pulp fibers, disk-like red blood cells and needle-like magnetic particulate recording media. The impact of particle shape through hydrodynamic interactions leads to a dynamic particle orientation distribution under flow. Jeffery (1922) demonstrated that an isolated

inertialess ellipsoid in an unbounded linear flow field undergoes a periodic closed orbit around the vorticity axis. The orbit period (T) of an ellipsoid with aspect ratio a_r (defined as major semi-axis length / minor semi-axis length) is given by,

$$T = \frac{2\pi}{\dot{\gamma}} \left(a_r + \frac{1}{a_r} \right), \tag{1}$$

where $\dot{\gamma}$ is shear rate. This result for a periodic closed orbit can be extended to any axisymmetric particle by employing effective aspect ratio [Bretherton (1962)]. The effective aspect ratio is determined from experiment or numerical simulation. For cylindrical shape, Trevelyan and Mason (1951) have experimentally estimated the effective aspect ratio to be approximately $0.7 \times a_r$. A similar particle-level simulation by Joung (2006) found the effective aspect ratio to be $0.714 \times a_r$.

For non-spherical particulate suspensions, particle-level simulation provides a convenient investigative platform to determine microstructure and the corresponding rheological properties. Claeys and Brady (1993a) developed the Stokesian Dynamics algorithm for prolate spheroid and calculated macroscopic suspension properties including diffusivity, permeability and suspension viscosity. However, the methodology incurs an increased mathematical complexity due to the particle shape and long-range hydrodynamic interactions. Yamane *et al.* (1994) employed a simplified model of rod-like particulate suspensions. Although hydrodynamic drag coefficients for rod-like particle were employed to account for near-field lubrication interactions, the long-range hydrodynamic effect was ignored. The authors validated the proposed model by demonstrating a good agreement in viscosity of isotropic suspension with that calculated by Claeys and Brady (1993b). However, Fan *et al.* (1998) demonstrated that the long-range hydrodynamic interactions are important. The authors employed a slender body assumption to account for the long-range part of hydrodynamic interaction. The shear-induced Folgar-Tucker diffusion constants obtained by their simulations are comparable to values obtained by experiments [Folgar and Tucker (1984)], and the magnitude of the diffusion constants from both studies are much higher than that of Yamane *et al.* (1994) which included only near-field contributions.

An alternative strategy of modeling non-spherical particles by numerous smaller spheres rigidly connected to each other, has been previously explored [Yamamoto and Matsuoka (1993); Kutteh (2003); Joung (2006); Meng and Higdon (2008)]. Yamamoto and Matsuoka (1993) proposed a method to

model a non-spherical particle by a group of bonded spheres. The stretching, bending and twisting deformation modes were taken into account for each connected sphere pair. Pairwise hydrodynamic interactions between clusters were employed . However, only the near-field squeezing-mode lubrication was included to characterize the hydrodynamic interaction of spheres within the same cluster. Their proposed methodology was employed in the subsequent studies of rod-like particulate suspension [Yamamoto and Matsuoka (1995)] and plate-like particulate suspension [Yamamoto and Matsuoka (1997)]. Rod-like particles are initially observed to be aligned in the shear direction. However, the presence of particles oriented along the vorticity direction become noticeable at later time. Simulation results using a similar approach by Lindstrom and Uesaka (2008) also showed a similar tendency.

Joung (2006) proposed a particle-level simulation method similar to the model of Yamamoto and Matsuoka (1993). However, the rod-like particle was modeled by three-dimensional spheres subjected only to stretching deformation at each joint. This model correctly predicted the dynamics of an isolated rod-like and plate-like particle in shear flow.

In this article, the concept proposed by Joung (2006) is extended to predict rheology and microstructure of non-spherical particulate suspensions in a simple shear flow. The details of the simulation method and the evaluation of microstructure and relevant rheological properties are described below. The results section begins with a discussion of an isolated rod-like particle in the simple shear flow for the purpose of model validation. The period of Jeffery orbits obtained by the model is compared with available literature results. This is followed by simulations of non-spherical particulate suspensions. The formation of lamellar structures at small Mason numbers and the impact on transient rheological properties are investigated. The orientation distribution of particles obtained from the model quantitatively agrees with the experimental results of Stover *et al.* (1992). Shear viscosity evaluated by orientation distribution is in quantitative agreement with that obtained using direct computation of particle stress, within statistical uncertainty.

3 Simulation method

Following the idea proposed by Joung (2006), a cubic building block for a non-spherical particle is made of a collection of equal-size spheres of radius a connected by bonds as shown in Fig. 1(a). Each subunit is composed of a

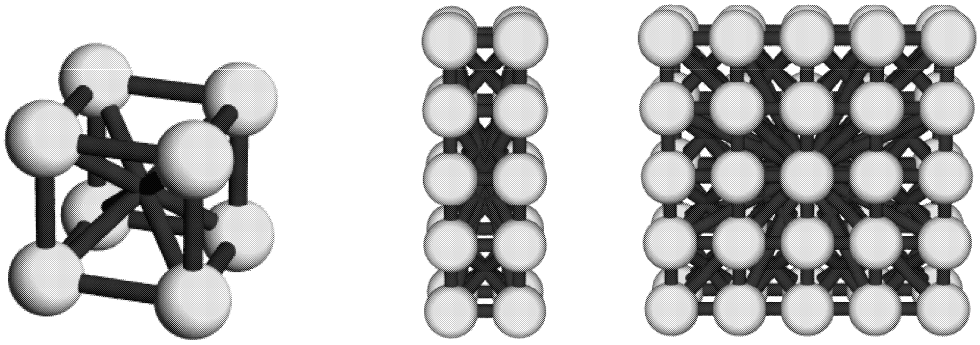

(a) subunit (b) rod-like and plate-like particle

Figure 1: A schematic diagram of non-spherical particle made of linked spheres

four-sphere forming a cube of side length $5a$. These cubic subunits are stacked together to form non-spherical particle as illustrated in Fig. 1(b) for rod-like and plate-like particles. There are additional bonds linking each sphere to the particle's center of mass to facilitate rigid body motion. The aspect ratio (a_r) of non-spherical particle is evaluated as the ratio of particle enveloped length per equivalent diameter [Joung (2006)]. The equivalent diameter (d_{eq}) is taken to be a diameter of a circle which has the same cross-sectional area to that of particle cross-sectional area which has its normal vector parallel to the principal axis.

Each sphere pair is linked together along the line of centers by Hookean links. Consider a pair of spheres α and β separated by a distance $r_{\alpha\beta} = ||\boldsymbol{r}_\beta - \boldsymbol{r}_\alpha||$. At each joint, only the linkage force along the line of centers is determined. While the bending and twisting modes are ignored, angular motion of the particle including Jeffery elliptic and axial spin orbit can be reproduced using this simplified linkage force model [Joung (2003)]. This is attributed to the three-dimensional linkage construction of a rod-like particle. The linkage force along the line of centers $\boldsymbol{F}_{\alpha\beta}^{\mathrm{link}}$ on sphere α due to a linkage with sphere β is given by,

$$\boldsymbol{F}_{\alpha\beta}^{\mathrm{link}} = k(r_{\alpha\beta} - r_{\alpha\beta}^{\mathrm{eq}})\boldsymbol{e}_r, \tag{2}$$

where k is the extensional-mode stiffness coefficient, r^{eq} is the equilibrium particle-particle separation distance and $\boldsymbol{e}_r$ is a unit vector along the line of from the center of sphere α to the center of sphere β. In this study,

$k = 100$ is employed. Since the stiffness coefficient is finite, the sphere cluster is approximately a rigid particle. Joung (2006) employed $k = 30 - 50$ in his investigation and found no apparent deformation with the sphere pairs deflection distance ($|r - r^{\mathrm{eq}}|/r^{\mathrm{eq}}$) never exceeds 1%.

Suspensions are composed of rod-like particles constructed as above, dispersed in a Newtonian suspending fluid of viscosity η_c. Suspensions are exposed to a linear shear flow with a shear rate magnitude $\dot{\gamma}$. Each sphere in the subunit is considered non-Brownian, neutrally-buoyant and inertialess. In the limit of vanishing particle and fluid inertia, sphere motions are determined by the balance of hydrodynamic force($\boldsymbol{F}^{\mathrm{Hyd}}$) and non-hydrodynamic force ($\boldsymbol{F}^{P}$) acting on each sphere. The governing equation of sphere α is written as,

$$\boldsymbol{F}_{\alpha}^{P} + \boldsymbol{F}_{\alpha}^{\mathrm{Hyd}} = 0. \tag{3}$$

Two types of non-hydrodynamic forces are considered in the model. First, the linkage force ($\boldsymbol{F}^{\mathrm{link}}$) acting on the linkage joint at sphere center is described in Eq. 2. The other non-hydrodynamic force is a short-range repulsive force ($\boldsymbol{F}^{\mathrm{rep}}$). The presence of repulsive force is necessary to prevent overlapping between particles due to the lack of lubrication force (which will be discussed later). The $\boldsymbol{F}_{\alpha\beta}^{\mathrm{rep}}$ on sphere α due to sphere β is written as,

$$\boldsymbol{F}_{\alpha\beta}^{\mathrm{rep}} = -F_{o}^{\mathrm{rep}} \frac{\exp(-\kappa(r_{\alpha\beta} - r_{\min}))}{1 - \exp(-\kappa(r_{\alpha\beta} - r_{\min}))}\, \boldsymbol{e}_{r}, \tag{4}$$

where κ^{-1} is the decay length, F_{o}^{rep} is the repulsive force magnitude and $r_{\min} = 2a$ is the minimum particle-particle separation distance. In this study, $F_{o}^{\mathrm{rep}} = 6\pi\eta_c\dot{\gamma}a^2$ for simulation in simple shear flow where $\dot{\gamma}$ denotes shear rate. Thus, the non-hydrodynamic force is the sum of these two contributions: $\boldsymbol{F}_{\alpha}^{P} = \sum_{\beta''} \boldsymbol{F}_{\alpha\beta''}^{\mathrm{link}} + \sum_{\beta'} \boldsymbol{F}_{\alpha\beta'}^{\mathrm{rep}}$. The notations β'' and β' denote that spheres β belongs to the same / different cluster to that of sphere α, respectively.

From Faxen's law, the hydrodynamic force acting on sphere α can be written as,

$$\boldsymbol{F}_{\alpha}^{\mathrm{Hyd}} = 6\pi\eta_c a(\boldsymbol{U}^{\infty} - \boldsymbol{U}_{\alpha}) + 6\pi\eta_c a(1 + \frac{a^2}{6}\nabla^2)\boldsymbol{U}_{\alpha}^{\mathrm{dist}} \tag{5}$$

where $\boldsymbol{U}^{\infty}$, $\boldsymbol{U}_{\alpha}$ and $\boldsymbol{U}_{\alpha}^{\mathrm{dist}}$ are ambient velocity, velocity of sphere α and disturbance velocity evaluated at center of sphere α, respectively. The disturbance velocity is modeled to be the pairwise summation of far-field disturbance velocities. Employing the singularity solution to Stokes' flow [Kim and Karilla

(1991)], the 1st correction to disturbance velocity experienced by sphere α due to motion of sphere β is given by,

$$\boldsymbol{U}_{\alpha\beta}^{\mathrm{dist},(0)} = (1 + \frac{a^2}{6}\nabla^2)\frac{\mathcal{G}(\boldsymbol{x}_\beta - \boldsymbol{x}_\alpha)}{8\pi\eta_c} \cdot \boldsymbol{F}_\beta^{\mathrm{Hyd},(0)}, \tag{6}$$

where $\mathcal{G} = r^{-1}(\boldsymbol{\delta}+\boldsymbol{e}_r\boldsymbol{e}_r)$ is the Oseen tensor. The term $\boldsymbol{F}_\beta^{\mathrm{Hyd},(0)} = 6\pi\eta_c a(\boldsymbol{U}^\infty - \boldsymbol{U}_\beta)$ is the hydrodynamic force on isolated sphere β, and is equivalent to Stokes drag force. Total disturbance velocity is treated to be equivalent to the sum of the disturbance field generated by all other sphere in the system. Additional correction terms to the disturbance field can be obtained iteratively by including the correction to the particle velocity to calculate new hydrodynamic force acting on sphere β, and the subsequent new correction to velocity disturbance field [Kim and Karilla (1991)]. Here, only the 1st correction will be included. Substituting Eq. 6 into Eq. 5, the hydrodynamic force on sphere α becomes,

$$\begin{aligned}
\frac{\boldsymbol{F}_\alpha^{\mathrm{Hyd}}}{6\pi\eta_c a} &= (\boldsymbol{U}^\infty - \boldsymbol{U}_\alpha) + \sum_{\alpha\neq\beta}(1 + \frac{a^2}{6}\nabla^2)^2\frac{\mathcal{G}(\boldsymbol{r}_{\alpha\beta})}{8\pi\eta_c} \cdot 6\pi\eta_c a(\boldsymbol{U}^\infty - \boldsymbol{U}_\beta), \quad (7)\\
&= (\boldsymbol{U}^\infty - \boldsymbol{U}_\alpha) + \sum_{\alpha\neq\beta}\mathbf{M}_{\alpha\beta}^{\mathrm{RP}} \cdot (\boldsymbol{U}^\infty - \boldsymbol{U}_\beta), \quad (8)
\end{aligned}$$

where $\mathbf{M}^{\mathrm{RP}}$ is the Rotne-Prager tensor describing far-field hydrodynamic interactions and is expressed as,

$$\mathbf{M}_{\alpha\beta}^{\mathrm{RP}} = \frac{3a}{4r}\left(\boldsymbol{\delta} + \boldsymbol{e}_r\boldsymbol{e}_r\right) + \frac{a^3}{2r^3}\left(\boldsymbol{\delta} - 3\boldsymbol{e}_r\boldsymbol{e}_r\right). \tag{9}$$

Here, $\boldsymbol{\delta}$ denotes Kronecker delta function, $r = ||\boldsymbol{x}_\beta - \boldsymbol{x}_\alpha||$, is a separation between sphere α (origin) and sphere β and $\boldsymbol{e}_r = \boldsymbol{r}/r$.

The absence of near-field lubrication is not expected to alter qualitative features of hydrodynamics. The short-range repulsive force in Eq. 4 exhibits diverging resistance in the limit of vanishing separation distance which is qualitatively similar to the near-field lubrication force due to squeezing flow.

The governing equation of sphere α motion can be obtained in a form suitable for particle-level simulation by substituting Eqs. 8–9 into Eq. 3:

$$\boldsymbol{U}_\alpha = \boldsymbol{U}^\infty + (6\pi\eta_c a)^{-1}\boldsymbol{F}_\alpha^P + \sum_{\alpha\neq\beta}^{N}\mathbf{M}_{\alpha\beta}^{\mathrm{RP}} \cdot (\boldsymbol{U}^\infty - \boldsymbol{U}_\beta). \tag{10}$$

To improve computational time [Sierou and Brady (2002)], the velocity of prior time step is employed as an approximation to the predicted value of $\boldsymbol{U}_\beta$). Sphere trajectories are determined by numerically integrating the above expression. While the hydrodynamics tensor in Eq. 9 can be directly applied in a particular situation such as monolayer simulation, an absolutely convergent form must be employed to a model system with periodic boundaries. The problematic long-range artifact can be resolved by a renormalization technique [O'Brien (1979)]. Beenakker (1986) has provided the Ewald summed form of $\mathbf{M}^{\mathrm{RP}}$ which is absolutely convergent. The synopsis of the procedure are as follows.

The rapidly converging Ewald sum of RP tensor composes of two contributions: $\mathbf{M}^{(1),\mathrm{RP}}$ and $\mathbf{M}^{(2),\mathrm{RP}}$ representing summation (of hydrodynamics interaction) in real and reciprocal space, respectively and are written as,

$$\begin{aligned} 6\pi\eta_{\mathrm{c}}a\mathbf{M}^{\mathrm{RP}} &= \sum_{l=1}^{\mathrm{Ncell}}{\sum_{\alpha\beta}}' \mathbf{M}^{(1),\mathrm{RP}}(\boldsymbol{r}_{\alpha\beta}) - \mathbf{M}^{(2),\mathrm{RP}}(\boldsymbol{r}=0) \\ &+ \frac{1}{V}\sum_{l^*=1}^{\mathrm{Ncell}}\sum_{\alpha\beta}\cos(\boldsymbol{k}_{\alpha\beta}\cdot\boldsymbol{r}_{\alpha\beta})\mathbf{M}^{(2),\mathrm{RP}}(\boldsymbol{k}_{\alpha\beta}). \end{aligned} \tag{11}$$

Here, the summation are conducted between sphere α in the main cell (containing N spheres) and sphere β which is located either in the main cell or in the surrounding periodic replicated cells. The $'$ notation on the $\mathbf{M}^{(1),\mathrm{RP}}$ summation indicates the exclusion of self-term ($\alpha=\beta$) when sphere β is in the main cell. Also, $l^*=1$ notation denotes that the reciprocal space summation excludes the case when interactions are within the main cell. The reciprocal lattice vector ($\boldsymbol{k}_{\alpha\beta}$) is related to the lattice vector $\boldsymbol{r}_{\alpha\beta}$ by $\exp(i\boldsymbol{k}_{\alpha\beta}\cdot\boldsymbol{r}_{\alpha\beta})=1$ and ξ is a parameter characterizing the distribution between real and reciprocal space summation. Here, $\xi=\sqrt{\pi}/V^{1/3}$ as proposed by Beenakker (1986). Also, the $\mathbf{M}^{(2),\mathrm{RP}}(\boldsymbol{r}=0)$ term on the R.H.S. of Eq. 11 is the reciprocal space contribution of the self-term ($\boldsymbol{r}=0$). Finally, $\mathbf{M}^{(1),\mathrm{RP}}(\boldsymbol{r})$,

$\mathbf{M}^{(2),\mathrm{RP}}(\boldsymbol{r}=0)$ and $\mathbf{M}^{(2),\mathrm{RP}}(\boldsymbol{k})$ are given by,

$$\begin{aligned}
\mathbf{M}^{(1),\mathrm{RP}}(\boldsymbol{r}) &= \left(\frac{3}{4}a+\frac{1}{4}a^3\nabla^2\right)\left(\boldsymbol{\delta}\nabla^2-\boldsymbol{\nabla}\boldsymbol{\nabla}\right) r\ \mathrm{erfc}(r\xi), && (12)\\
\mathbf{M}^{(2),\mathrm{RP}}(\boldsymbol{r}=0) &= \boldsymbol{\delta}(\frac{6}{\sqrt{\pi}}\xi a-\frac{40}{3\sqrt{\pi}}\xi^3a^3), && (13)\\
\mathbf{M}^{(2),\mathrm{RP}}(\boldsymbol{k}) &= (\boldsymbol{\delta}-\boldsymbol{e}_k\boldsymbol{e}_k)\left(a-\frac{1}{3}a^3k^2\right)\left(1+\frac{1}{4}\frac{k^2}{\xi^2}+\frac{1}{8}\frac{k^4}{\xi^4}\right)\\
&\times\ \frac{6\sqrt{\pi}}{k^2}\exp(-\frac{\xi^2k^2}{4}). && (14)
\end{aligned}$$

The governing equation is non-dimensionalized by the following scale variables:

$$L_s=a,\quad F_s=6\pi\mu_c\dot{\gamma}a^2,\quad t_s=\dot{\gamma}^{-1}, \tag{15}$$

Initial isotropic configurations are randomly generated. Particle configurations are saved every strain of 0.02 and shear viscosity is evaluated from these saved configurations.

The particle contribution to the shear stress is considered as a sum of two contribution:τ_{xy}^{hyd} and $\tau_{xy}^{\text{non-hyd}}$. The hydrodynamic contribution to the shear stress is evaluated according to the Einstein relationship: $\tau_{xy}^{\mathrm{hyd}}=2.5\phi\dot{\gamma}$. The nonhydrodynamic contribution to the shear stress is given by

$$\tau_{xy}^{\text{non-hyd}}=-\frac{1}{V}\sum_i y_iF_{x,i}^P, \tag{16}$$

where $F_{x,i}^P$ is the x component of the nonhydrodynamic force on sphere i, y^i is the y coordinate of sphere i, and V is the simulation cell volume.

The other approach to evaluate shear stress is to employ constitutive equation [Fan *et al.* (1998)]. The shear stress is a function of orientation tensor $< P_x^2P_y^2 >$ and the stress can be written as

$$\tau_{xy}=\eta_c\dot{\gamma}(1+\phi f(\phi,a_r))< P_x^2P_y^2 >, \tag{17}$$

where the function $f(\phi,a_r)$ is given by

$$f=\frac{a_r^2\phi(2-\phi/G)}{4(ln(2a_r)-1.5)(1-\phi/G)^2}, \tag{18}$$

which the parameter G is 0.53-0.013a_r. Also η_c is the viscosity of continuous phase. In the following section, the proposed model here will be employed to simulate isolated rod-like particle and suspension of non-spherical particulate suspensions in simple shear flow.

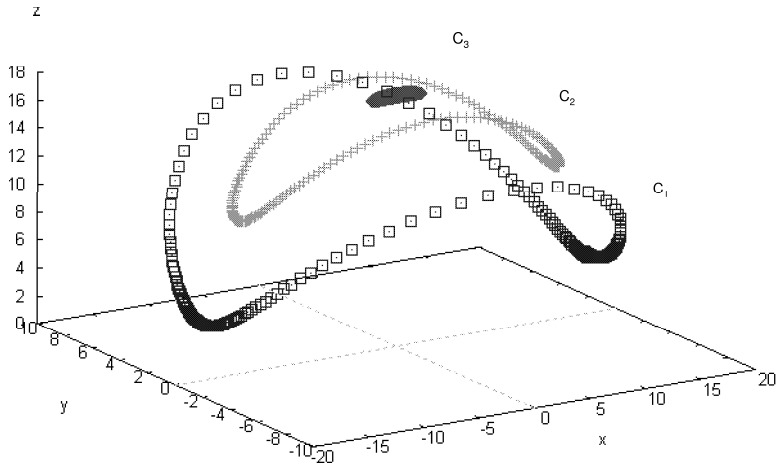

Figure 2: Simulated orbits of rigid rod-like particle with aspect ratio 4.43 at various orbit constants ($C_1 = 0.017455$, $C_2 = 0.1763$, $C_3 = 0.57737$)

4 Results

Representative trajectories for an isolated rod-like particle with aspect ratio 4.43 in simple shear flow are illustrated in Fig. 2. For an isolated particle simulation, there is no need to include repulsive force (Eq. 4) to prevent particle overlap. A change in particle initial orientations leads to a distinctly different closed orbit trajectory. The family of closed orbits can be characterized by an orbit constant C which is given by [Jeffery (1922)];

$$C = \frac{1}{a_r |P_z|} \sqrt{a_r^2 P_y^2 + P_x^2}, \tag{19}$$

where P_x, P_y and P_z are the flow, gradient and vorticity components of a unit vector parallel to particle principle axis. As illustrated in Fig. 2, an orbit will shift to rotation on flow-gradient plane as the orbit constant is increased. The trajectories in Fig. 2 are generated using a constant time interval. Dense data points along the flow axis (x direction) indicates the preferential orientation is in the flow direction.

The simulation period of rod-like particle is plotted as a function of aspect ratio in Fig. 3. Also, experimental results using glass cylinders reported by Trevelyan and Mason (1951) as well as numerical results by Skjetne *et al.* (1997), which modeled a rod-like particle as a linear chain of spheres with connectors, are given for a comparison. As discussed in the Introduction

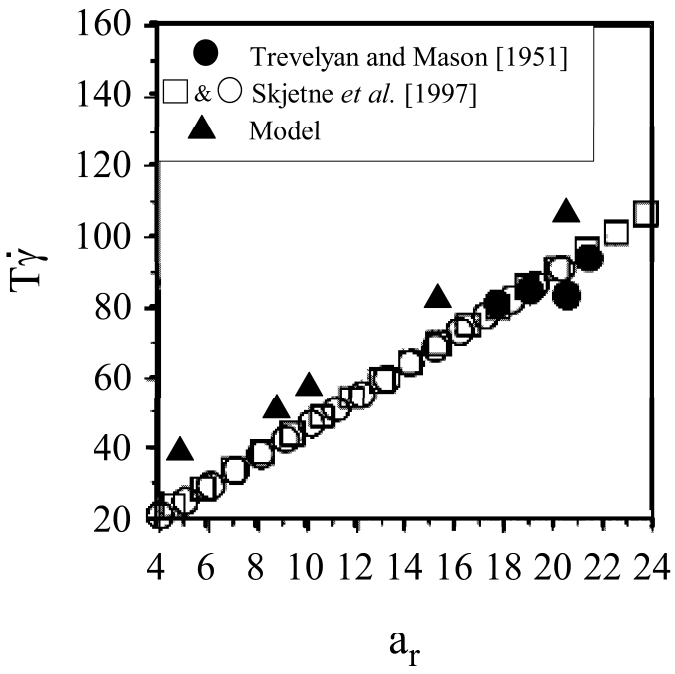

Figure 3: Orbit period of cylindrical rod as a function of aspect ratio. Linked-sphere model results represented by filled triangles are compared with numerical results reported Skjetne *et al.* (1997) (denoted by open circles and open squares) and experimental results reported by Trevelyan and Mason (1951) (denoted by filled circles).

section, the orbit period is described by Eq. 1 and is independent of initial orientation. In Fig. 3, the orbit periods increase with aspect ratio in a manner consistent with literature results. Some quantitative differences are expected due to the usage of the linked-sphere structure to represent a cylindrical body. However, the model demonstrates a good agreement with experimental results at large aspect ratio. Also, the additional length scale corresponding to the axisymmetric distribution of spheres clearly results in deviation from the simulation results reported by Skjetne *et al.* (1997) where the elongated particle is modeled as a line distribution of spheres. The exact contribution of these two causes is unclear. A better agreement to literature results could have been made by employing an effective aspect ratio in lieu of actual aspect ratio [Petrich *et al.* (2000)]. However, the actual aspect ratio will be used in this study.

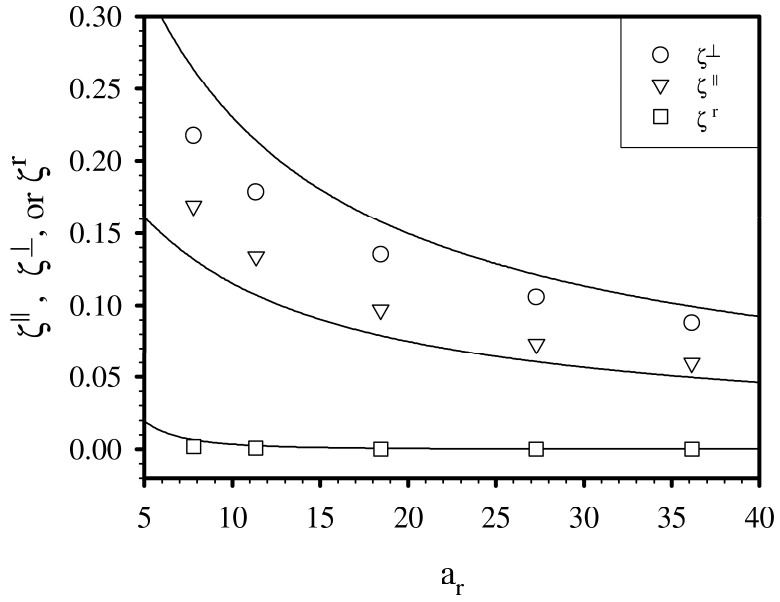

Figure 4: Longitudinal and transverse components of rod-shape friction tensor as a function of aspect ratio. Model results are compared with slender-body theoretical results given by Doi and Edwards (1986).

In Fig. 4, the components of translational drag coefficients and rotational viscous drag coefficient of an isolated rod-like particle in quiescent fluid is plotted as a function of particle aspect ratio. The theoretical value based on the slender body assumption [Doi and Edwards (1986)] is also included in Fig. 4 for comparison. The drag coefficient is defined as a ratio of translation/rotation velocity to body force/torque and is calculated from the simulation by monitoring particle velocity/angular velocity upon imposing known force/torque. The translation viscous drag is composed of two components: (1) drag for the motion along the line of centers ($\zeta^{||}$) and (2) drag for the motion perpendicular to the principal axis ($\zeta^{\perp}$). As demonstrated in Fig. 4, the transverse component drag coefficient from simulations is always higher than the line of centers component coefficient. The simulation results exhibit the trend of decreasing drag coefficients with increasing aspect ratio and is in a reasonable agreement with slender body results. However, the apparent difference between rod-like linked-sphere structure and cylindrical object lead to some quantitative difference to slender body results.

The particle orientation is monitored in terms of the normalized configu-

ration function [Fan *et al.* (1998)]. The flow (ζ) and vorticity (ξ) component of the configuration function is computed directly from particle orientation unit vector $\boldsymbol{P}$ and is given by

$$\zeta = \langle \frac{P_x^2}{P_x^2 + P_y^2} \rangle, \tag{20}$$

$$\xi = \langle \frac{P_z^2}{P_z^2 + P_x^2} \rangle. \tag{21}$$

In Fig. 5, ζ and ξ configuration function are plotted as a function of strain for rod-like suspensions with three different box sizes (or number of clusters). Here, the rod-like particle concentration is referred using the quantity nL^3, where L is the length of the elongated object and n is the number density. Particle aspect ratio is set to 2.48 and $nL^3 = 1$ in all simulations. Both ζ and ξ configuration function exhibit a cyclical variation which indicate particle motions follow Jeffery orbit [Yamane *et al.* (1994) and Fan *et al.* (1998)]. At this particular concentration, the structured evolution is insensitive to the change in box size over the observed length scale and there is no apparent transient structure changes over the observed time scale. Fan *et al.* (1998) reported a transient structured evolution at longer time scale and for certain particle concentration. However, the primary focus of this study will be restricted to the early stage of evolution during which there are no apparent transient structured changes.

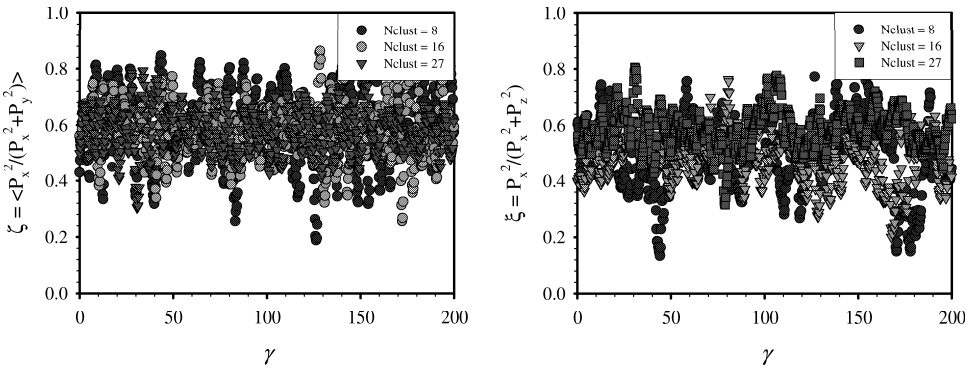

(a) Flow component (b) Vorticity component

Figure 5: Normalized flow and vorticity components of rod-like particle orientation as a function of strain ($a_r = 2.48$, $nL^3 = 1$).

An alternative way to characterize structured evolution is by monitoring the Jeffery orbit constant given in Eq. 19. The orbit constant has a range from zero, corresponding to particle oriented in vorticity direction, to infinity, corresponding to particle lying in flow-gradient plane. Thus, it is more convenient to recast the orbit constant in the form of $C_b = C/(1+C)$ which has the range between 0 and 1 instead. The distribution of orbit constant for a rod-like suspension wih $a_r = 11.34$ and $nL^3 = 1$ is shown in Fig. 6. Here, the differential of cumulative probability $P(C_b)$ with respect to the orbit constant $(\partial P(C_b)/\partial C_b)$ is calculated from simulation and compared with experimental results given by Stover *et al.* (1992) and Anczurowski and Mason (1967). It is apparent that the presence of hydrodynamics is necessary to reproduce the distribution of orbit constant in a consistent manner to the experimental results. A similar skewed C_b distribution is observed when particle concentration (nL^3) is varied. There is no distinct tendency of statistical mode and mean value of C_b with respect to concentration and aspect ratio over the observed range. This was also reported in simulation by Lindstrom and Uesaka (2008).

In Fig. 7, the normalized particle contribution to shear viscosity $((\eta_{\mathrm{xy}} - \eta_c)/\eta_c)$ of rod-like suspensions is plotted as a function of volume fraction. Here, $nL^3 = 1$ is fixed while particle aspect ratio is varied from 2.3 to 20.20. Shear viscosity is obtained by the direct stress calculation according to Eq. 16, and is in a good agreement with that obtained by the particle orientation configuration approach as in Eq. 17. Also, results are in good agreement with simulation results reported by Lindstrom and Uesaka (2008).

Simulation results for plate-like suspensions are presented in Figs. 8-9. The plate-like particle has a tendency to align its largest surface parallel to the shear flow as commonly observed [Yamamoto and Matsuoka (1997); Joung (2006); Meng and Higdon (2008)]. Here, the orientation vector is defined as a unit normal vector of the largest surface. Similar to the rod-like particle investigation, the distribution of differential orbit constants are evaluated for plate-like suspensions with aspect ratio 1/2.26 and $nL^3 = 1$. In Fig. 8, the differential probability distribution is compared with the experimental results by Anczurowski and Mason (1967) for a disc-like suspension with $a_r = 0.32$. Both data sets indicate a shift toward larger orbit constants corresponding to the largest surface lying on the shear-gradient plane.

Shear viscosity of plate-like suspensions $(1/a_r = 2.26)$ is plotted as a function of volume fraction in Fig. 9. The shear viscosity computed by direct stress calculation is in a reasonable agreement to that obtained by

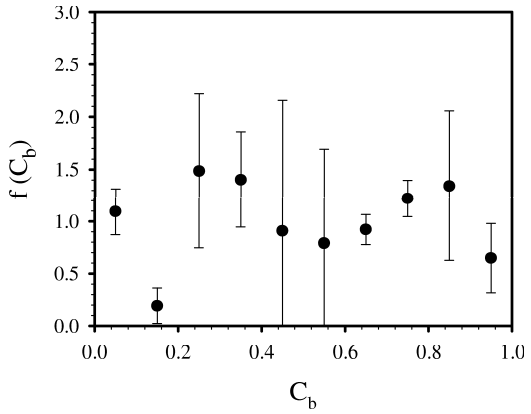

(a) Free-draining model

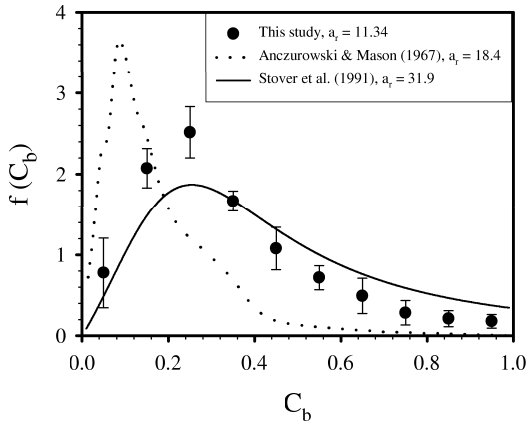

(b) Hydrodynamic model

Figure 6: Differential orbit constants distribution for rod-like suspension with and without hydrodynamic interactions ($a_r = 11.34$, $nL^3 = 1$).

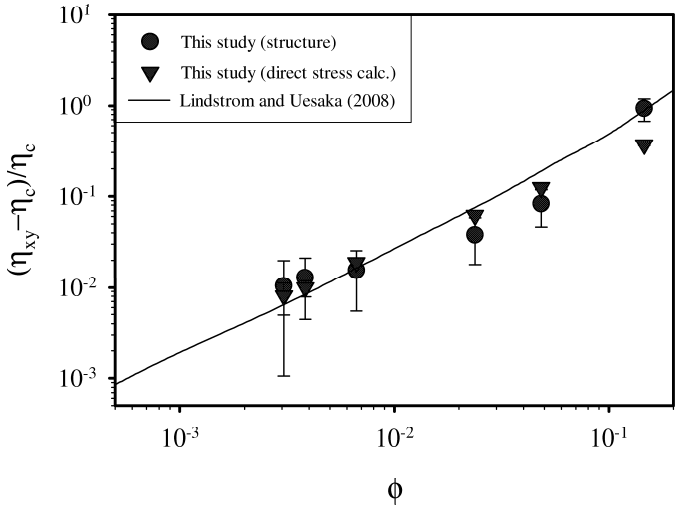

Figure 7: Particle contribution to viscosity of rod-like suspension as a function of volume fraction ($a_r = 2.3 - 20.20$, $nL^3 = 1$).

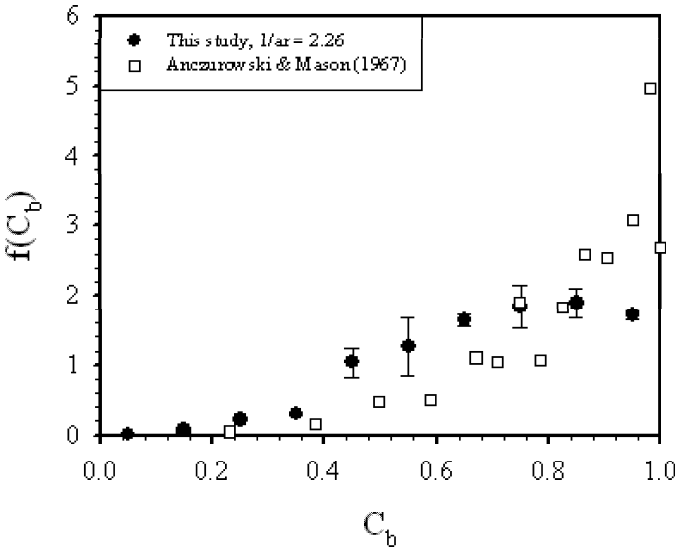

Figure 8: Differential orbit constants distribution for disc-like suspension ($a_r = 1/2.26$, $nL^3 = 1$). Experimental results ($a_r = 1/3$) by Anczurowski and Mason (1967) is given for comparison.

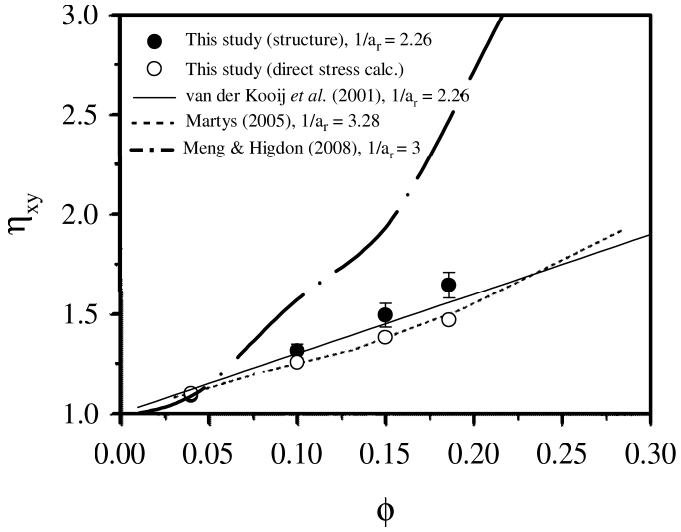

Figure 9: Shear viscosity of disc-like suspension as a function of volume fraction ($a_r = 1/2.26$). The solid line is the theoretical expression given by van der Kooij *et al.* (2001) ($a_r = 1/2.26$) The dash line represents simulation results of oblate spheroidal suspensions ($a_r = 1/3.28$) reported by Martys (2005) and the dash-dot-dash line is simulation results reported by Meng and Higdon (2008).

orientation distribution [Hinch and Leal (1972)]. Also in Fig. 9, a theoretical expression in the dilute limit using $1/a_r = 2.26$ [van der Kooij *et al.* (2001)], DPD simulation results ($1/a_r = 3.28$) by Martys (2005) and particle-level simulation of plate-like particle ($1/a_r = 3$) by Meng and Higdon (2008) are given. Qualitatively, shear viscosity monotonically increase as a function of volume fraction. Our simulation results agree well with the dilute theoretical expression. However, the predicted viscosity is smaller than the results of Meng and Higdon (2008) when ϕ becomes greater than 0.05. There is no clear explanation to the difference between our results and Meng and Higdon (2008). However, this is partly attributed to the flatter (high $1/a_r$) particle employed by Meng and Higdon (2008). In addition, the enveloped volume of sphere cluster is chosen to be particle volume. Consequently, this choice lead to lower effective particle volume due to consideration amount of gap volume among spheres. However these factors are not expected to produce such a significant difference. Available literature results reveal somewhat discrepancy of viscosity values even at low to moderate volume fraction. In Fig. 9, the magnitude by DPD simulation of ellipsoidal suspensions by Martys (2005) is smaller than values reported by Meng and Higdon (2008). Subsequent works particularly that related to experimental measurements will be instructive.

5 Conclusion

In this study, a simple approach to modelling a non-spherical particle in a Newtonian fluid is presented by considering the particle to be composed of spheres connected by Hookean constraint forces acting along the line-of-center direction. The three-dimensional cluster structure allow the exclusion of bending and twisting forces at each joint. Rotne-Prager correction to velocity disturbance has been employed to account for far-field hydrodynamic interactions. Simulations of isolated rod-like and plate-like particle in simple shear flow produced a periodic orientation distribution (Jefferys orbit). The period of Jeffery's orbit as a function of aspect ratio quantitatively agree with literature results. Particle drag coefficient is in good agreement with slender-body theoretical results.

Rheology of non-colloidal non-spherical suspensions in simple shear flow has been investigated. Short-range repulsive force is included to model non-spherical particulate suspensions. As a first step to explore capability and limitation of the proposed algorithm, the relatively well understood rod-like

suspensions and plate-like suspensions were investigated. The model produces microstructure which qualitatively agrees with experimental results by Stover *et al.* (1992) and Anczurowski and Mason (1967). The presence of long-range hydrodynamics is necessary to produce microstructure in a manner consistent with experimental observations. This linked spheres method offers another useful investigative tool to visualize the dynamics of various particle type. Although the primary focus of this study is on rigid particle, preliminary results have demonstrated the model feasibility to capture flexible fiber configuration dynamics such as S-turn in simple shear.

Rheological properties have been evaluated by two different approaches: orientation distribution and direct computation of particle stress. Shear viscosity at low to moderate volume fraction corresponding to dilute to semi-dilute regime is of a particular interests. Shear viscosity of rod-like as well as plate-like suspensions evaluated by both approaches are in good agreement and compare well with available literature results.

6 Acknowledgements

This work was supported in part by Australian Research Council (Discovery Project no. DP0666004). Authors are grateful for helpful comments by Prof. Roger I. Tanner, Prof. Xijun Fan, Dr. Clint Joung and Mr. Erwan Bertevas.

References

Anczurowski, E. and S. G. Mason, "The kinetics of flowing dispersions iii. equilibrium orientations of rods and discs (experimental)," J. Colloid INterface Sci. **23**, 533–546 (1967).

Beenakker, C. W. J., "Ewald sum of the rotne-prager tensor," J. Chem. Phys. **85**, 1581–1582 (1986).

Bretherton, F. P., "The motion of rigid particles in a shear flow at low reynolds number," J. Fluid Mech. **14**, 284–304 (1962).

Claeys, I. L. and J. F. Brady, "Suspensions of prolate spheroids in stokes flow. part 1. dynamics of a finite number of particles in an unbounded fluid," J. Fluid Mech. **251**, 411–442 (1993a).

Claeys, I. L. and J. F. Brady, "Suspensions of prolate spheroids in stokes flow. part 2. statistically homogeneous dispersions," J. Fluid Mech. **251**, 443–477 (1993b).

Doi, M. and S. F. Edwards, *The theory of polymer dynamics*, Clarendon Press, London (1986).

Fan, X., N. Phan-Thien and R. Zheng, "A direct simulation of fibre suspensions," J. Non-Newtonian Fluid Mech. **74**, 113–135 (1998).

Folgar, F. and C. L. Tucker, "Orientation behavior of fibers in concentrated suspensions," J. Reinf. Plastics Composites **3**, 98–119 (1984).

Hinch, E. J. and L. G. Leal, "The effect of brownian motion on the rheological properties of a suspension of non-spherial particles," J. Fluid Mech. **52**, 683–712 (1972).

Jeffery, G. B., "Motion of ellipsoidal paritcles immersed in a viscous fluid," Proc. R. Soc. Londdon Ser. A **102**, 161–179 (1922).

Joung, C. G., *Direct Simulation Studies of Suspended Particles and Fibre-filled Suspensions*, Ph.D. thesis, University of Sydney (2003).

Joung, C. G., "Dynamic simulation of arbitrarily shaped particles in shear flow," Rheol. Acta **46**, 143–152 (2006).

Kim, S. and S. J. Karilla, *Microhydrodynamics*, Butterworth- Heinemann, London (1991).

Kutteh, R., "Stokesian dynamics of nonspherical particles, chains and aggregates," J. Chem. Phys. **119**, 9280–9294 (2003).

Lindstrom, S. B. and T. Uesaka, "Simulation of semidilute suspensions of non-brownian fibers in shear flow," J. Chem. Phys. **128**, 024901–14 (2008).

Martys, N. S., "Study of a dissipative particle dynamics based approach for modeling suspensions," J. Rheol. **49**, 401–424 (2005).

Meng, Q. and J. J. Higdon, "Large scale dynamic simulation of plate-like particle suspensions. part i: Non-brownian simulation," J. Rheol. **52**, 1–36 (2008).

O'Brien, R. W., "A method for the calculation of the effective transport properties of suspensions of interacting particles," J. Fluid Mech. **91**, 17–39 (1979).

Petrich, M. P., D. L. Koch and C. Cohen, "An experimental determination of the stress-microstructure relationship in semi-concentrated fiber suspensions," J. Non-Newtonian Fluid Mech. **95**, 101–133 (2000).

Sierou, A. and J. F. Brady, "Rheology and microstructure in concentrated noncolloidal suspensions," J. Rheol. **46**, 1031–1056 (2002).

Skjetne, P., R. F. Ross and D. J. Klingenberg, "Simulation of single fiber dynamics," J. Chem. Phys. **6**, 2108–2121 (1997).

Stover, C. A., D. L. Koch and C. Cohen, "Observations of fibre orientation in simple shear flow of semi-dilute suspensions," J. Fluid Mech. **238**, 277–296 (1992).

Trevelyan, B. J. and S. G. Mason, "Particle motion in sheared suspensions," J. Colloid. Sci. **6**, 354 (1951).

van der Kooij, F. M., E. S. Boek and A. P. Philipse, "Rheology of dilute suspensions of hard platelike colloids," J. Colloid. Sci. **235**, 344–349 (2001).

Yamamoto, S. and T. Matsuoka, "A method for dynamic simulation of rigid and flexible fibers in a flow field," J. Chem. Phys. **98**, 644–650 (1993).

Yamamoto, S. and T. Matsuoka, "Dynamic simulation of fiber suspensions in shear flow," J. Chem. Phys. **102**, 2254–2260 (1995).

Yamamoto, S. and T. Matsuoka, "Dynamic simulation of a platelike particle dispersed system," J. Chem. Phys. **107**, 3300–3308 (1997).

Yamane, Y., Y. Kaneda and M. Doi, "Numerical simulation of semi-dilute suspensions of rodlike particles in shear flow," J. Non-Newtonian Fluid Mech. **54**, 405–421 (1994).